Electron-phonon Coupling in the $^4T_{2g}$ Excited Electron State of Cs_2GeF_6:Mn^{4+}

N. M. Avram and M. G. Brik[a]

Department of Physics, West University of Timisoara, Bd. V. Parvan 4, Timisoara 300223, Romania
[a] Fukui Institute for Fundamental Chemistry, Kyoto University, 34–4, Takano Nishihiraki-cho, Sakyo- ku, Kyoto 606–8103, Japan

Reprint requests to Dr. M. G. B., e-mail brik@fukui.kyoto-u.ac.jp

Z. Naturforsch. **60a,** 54 – 60 (2005); received September 18, 2004

In the present paper we report on an analysis of the fine structure of the first excited quartet $^4T_{2g}$ of Mn^{4+} ions which occupy the octahedral site in the Cs_2GeF_6 host crystal. The dynamic $^4T_{2g} \otimes (e_g + t_{2g})$ Jahn–Teller effect is considered in details, including the Ham effect of the reduction of the spin-orbit splitting and displacements of the ligands due to the combined effect of the a_{1g} and e_g normal modes of the $[MnF_6]^{2-}$ octahedral complex. The electron-phonon coupling constants are evaluated using the experimental spectroscopic data. The value of the Jahn–Teller stabilization energy $E_{JT} = 438$ cm^{-1} for the considered complex is estimated from both the Ham effect and the potential energy surface of the $^4T_{2g}$ excited state.

Key words: Laser Crystals; Electron-phonon Coupling; Jahn–Teller Effect.

1. Introduction

Transition metal ions as optical active centers in various crystals have been the subject of a great number of experimental and theoretical studies (e. g. [1, 2] and references therein). Electronic transitions between the energy levels of their external unfilled 3d shell give rise to intense and broad (or sharp) luminescence bands depending on the spin and symmetry of the states involved in the transitions and the dynamics of the environment surrounding the active ions in the crystal.

The host materials doped with transitional metal ions with $3d^3$ electron configuration (V^{2+}, Cr^{3+} and Mn^{4+}) have received considerable attention, both experimental and theoretical, during the development of the crystal and ligand field theories [3 – 6]. The reason is that the $3d^3$ electron shell has a very attractive combination of spin-doublet and spin-quartet states in the octahedral crystal field, which allows for getting either sharp luminescence lines (in the case of a strong crystal field, when the first excited state is the ^2E_g doublet) or broadband luminescence (in the case of a weak crystal field with the $^4T_{2g}$ quartet being the first excited state). Among different possible hosts for these ions, chloride and fluoride crystals are especially interesting from the spectroscopic point of view, since the phonon cut-off energy is rather low, causing the emission life-time of the excited state to be greater than, for example, for oxides crystals.

V^{2+} ions typically show a high quantum efficiency of fluorescence in different host crystals. Their spectroscopic and lasing properties in doped halide crystals have been studied in [7 – 9]. Cr^{3+} ions as active centers in tunable laser materials and sensitizers in rare-earth co-doped host materials have been described in [10 – 12].

The vibronic spectra and lattice dynamics of $A_2{}^1M^{IV}F_6$:$MnF_6{}^{2-}$ compounds (A^1 = K, Rb, M^{IV} = Si; A^1 = Cs, M^{IV} = Si, Ge) have been investigated from both experimental and theoretical points of view [13 – 16]. All spectra of the V^{2+}, Cr^{3+} and Mn^{4+} ions in various crystals are strongly influenced by a coupling between the phonons of the host matrix and the electronic state of the impurity ion.

The vibronic interaction as dynamical Jahn–Teller effect in the $^4T_{2g}$ excited state has been investigated for different combinations of impurity ions and host crystals: by Sturge [17] for $KMgF_3$:V^{2+}, Bevilacqua et al. [18] for ZnS:V^{2+} and ZnSe:V^{2+}, Avram and Brik [19] for $CsCaF_3$:V^{2+}, Güdel and Snellgrove [20] for $Cs_2NaInCl_6$:Cr^{3+}, Pilla et al. [21] for $KZnF_3$:Cr^{3+}, Knochenmuss et al. [22] for $CsNaYCl_6$:Cr^{3+}, Wenger

and Güdel [23] for $CsNaScCl_6:Cr^{3+}$, Avram and Brik [24] for $LiCaAlF_6:Cr^{3+}$, Ring-Ling Chien et al. [15] for $Cs_2GeF_6:Mn^{4+}$. All these authors analyzed the Ham reduction [25] of spin-orbit splitting of the $^4T_{2g}$ excited state of the above-mentioned $3d^3$ ions. Studies of the $^4T_{2g}$ excited state geometry were made in [22, 23], resulting in the evaluation of the magnitudes of the ligands displacements and getting the potential energy surface cross-sections for the excited state. Avram et al. [26] have investigated the electron-phonon interaction in the $CsCaF_3:V^{2+}$ laser crystal and the geometry of the $[VF_6]^{4-}$ complex in the $^4T_{2g}$ excited state of the V^{2+} ion.

The aim of this paper is a theoretical analysis of the $^4T_{2g}$ excited state in $Cs_2GeF_6:Mn^{4+}$ crystal, with the main attention being paid to the geometry of this electronic state, influenced by its coupling with the total symmetric a_{1g} and double degenerated e_g normal vibrations of the $[MnF_6]^{2+}$ complex due to the dynamic Jahn–Teller effect. Such an analysis permits to estimate the changes of the chemical bond lengths due to the combined effect of the a_{1g} and e_g normal modes, plot the cross-sections of the potential energy surface as a function of the ionic displacements, and deduce the value of the Jahn–Teller stabilization energy. The results of this investigation are accurate because the $[MnF_6]^{2-}$ octahedron does not share faces, edges or corners with neighboring octahedra and is, therefore, weakly coupled to the lattice with quite sharp spectral features [16]. That is why the cluster model of Sturge [27], which treats an impurity center as an isolated molecule, can be used.

2. Experimental Support

The basis of our theoretical analysis will be the experimental energy data obtained from the optical spectra of the Cs_2GeF_6 crystals doped with Mn^{4+} ions. For this reason we present briefly in this section the results of the spectroscopic studies of Mn^{4+} centers in octahedral sites in Cs_2GeF_6 crystal carried out by Helmholtz and Russo [14], Chien et al. [15] and Campochiaro et al. [16].

Cs_2GeF_6 crystallizes in the Fm3m – $O_h{}^5$ (antifluorite) space group with the lattice constant $a = 3.60$ Å [13]. Each germanium ion occupies a position with O_h site symmetry and is surrounded by six fluorines at 1.80 Å distance. The $[MnF_6]^{2-}$ ion may be introduced as an impurity such one obtains the system Cs_2MnF_6, with the Mn – F distance equal 1.74 Å [14]. So, in this system, Mn^{4+} at Ge sites in Cs_2GeF_6 is octahedrally coordinated by F^- ions. The $[MnF_6]^{2-}$ unit has eight nearest – neighbor Cs^+ ions lying outward the octahedron faces and forming a cube. The weak coupling of the $[MnF_6]^{2-}$ unit to the rest of the lattice is readily justified by the following features: the sharpness of the vibrational lines, the near absence of lines due to $GeF_6{}^{2-}$ octahedra, the weakness of acoustic phonon bands, and the host independence of the spectra [15]. The Mn^{4+} ion has three 3d electrons in its ground state, and all its visible and near ultraviolet spectra are due to the d → d transitions, in an exact analogy to Cr^{3+} or V^{2+}. The one-photon spectrum consists of a weak magnetic dipole and some magnetic dipole sidebands, but is dominated by spectra based on the three odd parity modes of the $[MnF_6]^{2-}$ octahedron [14]. In [14] the $^4A_{2g} \rightarrow {}^4T_{2g}$ transition has been investigated by one photon spectroscopy, and it was shown that the $^4T_{2g}$ state undergoes spin-orbit splitting into Γ_7, $\Gamma_8{}^b$, Γ_6, $\Gamma_8{}^a$ components, in the order of increasing energy. The first three were identified at 20620.5, 20626.6 and 20636.5 cm^{-1}, with energies relative to that for the Γ_7 state having the values 0, 6.1, and 16 cm^{-1} respectively.

The two photon spectra of $Cs_2MF_6:Mn^{4+}$ have been observed by Chien et al. [15]. They have established the following fine structure of the $^4T_{2g}$ excited state: $\Gamma_7 : 0$, $\Gamma_8{}^b : 10.2$, $\Gamma_6 : 54$ and $\Gamma_8{}^a : 64$ cm^{-1} (all above 20625.8 cm^{-1}). An analysis of the Ham quenching for the $^4A_{2g} \rightarrow {}^4T_{2g}$ zero phonon line had also been made.

Campochiaro et al. [16] reported the low temperature (7 K) single crystal two photon spectra of the $^4A_{2g} \rightarrow {}^4T_{2g}$ transition in the $Cs_2GeF_6:Mn^{4+}$. They observed all four zero-phonon lines of the $^4A_{2g} \rightarrow {}^4T_{2g}$ transition, and the multiplet components are assigned as Γ_7 at 0 cm^{-1}, Γ_8 at 11 cm^{-1}, Γ_6 at 64 cm^{-1} and $\Gamma_8{}'$ at 74 cm^{-1}. They pointed out that the line at 54 cm^{-1} (assigned in [15] to Γ_6) is actually a lattice mode, not a quartet component.

3. The $^4A_{2g} \rightarrow {}^4T_{2g}$ Transition in a Static Crystal Field

The absorption zero-phonon line for the above transition in the $Cs_2GeF_6:Mn^{4+}$ crystal exhibits a fine structure resulting in four lines which correspond to the spin-orbit splitting of the $^4T_{2g}$ level. The 12-fold-degenerated $^4T_{2g}$ term is split by the spin-orbit interaction into four terms transforming as Γ_6, Γ_7, $\Gamma_8{}^a$, $\Gamma_8{}^b$ irre-

Table 1. The relative energy (in cm^{-1}) of the four spin-orbit components of the $^4T_{2g}$ state in Cs_2GeF_6:Mn^{4+}.

Γ	a	b	c
Γ_7	0	0	0
$\Gamma_8{}^a$	89	11	14.9
Γ_6	276	64	63.4
$\Gamma_8{}^b$	282	74	73.4

a) Calculation using the full d^3 matrix [28] with $Dq = 2063$ cm^{-1}, $B = 491$ cm^{-1}, $C = 4053$ cm^{-1} and $\xi_{SO} = 380$ cm^{-1}. b) Experimentally observed relative energies [16]. c) Calculation including the Jahn–Teller reduction parameter $\gamma = 0.26$.

ducible representations of the octahedral double group

$$^4T_{2g} \rightarrow \Gamma_6 + \Gamma_7 + \Gamma_8{}^a + \Gamma_8{}^b.$$

The full d^3 matrices of Eisenstein [28], including the spin-orbit interaction ($\xi_{SO} = 380$ cm^{-1} for Mn^{4+} [29]) were used to calculate the energies of the four $^4T_{2g}$ spinors in a perfect octahedral static crystal field. The values $Dq = 2063$ cm^{-1}, $B = 491$ cm^{-1} and $C = 4053$ cm^{-1} are chosen to fit the absorption spectra of the title system from paper [15]. The results are shown in Table 1, column a. A comparison with the experimental splitting in column b shows that the calculated overall spinors splitting is overestimated by more than a factor of 3.8. This discrepancy is unambiguously interpreted as a manifestation of the Jahn–Teller effect in the $^4T_{2g}$ state, which partially quenches the orbital angular momentum and reduces the total spin-orbit splitting (Ham effect [25]).

In order to model the observed spin-orbit splitting we used the second-order spin-orbit Hamiltonian [30]

$$H_{\text{eff}} = \lambda \vec{L}\vec{S} + k\left(\vec{L}\vec{S}\right)^2 + \rho(L_x^2 S_x^2 + L_y^2 S_y^2 + L_z^2 S_z^2) \quad (1)$$

acting in the space of 12 wave functions of the degenerate $^4T_{2g}$ state with $L = 1$ and $S = 3/2$. The values of the adjustable parameters λ, k and ρ are determined by fitting the eigenvalues of the H_{eff} matrix to the $^4T_{2g}$ spinor splitting calculated with the full d^3 matrices (column a in Table 1). We obtained $\lambda = 73.60$, $k = 2.93$ and $\rho = 3.32$ (all in cm^{-1}).

4. Electron-phonon Coupling in the $^4T_{2g}$ Excited State

The Hamiltonian for the Mn^{4+} ion in the octahedral crystal field of Cs_2GeF_6 can be written as

$$H = H_{\text{FI}} + H_{\text{CF}} + H_{\text{SO}} + H_{\text{VIB}}. \quad (2)$$

The first three terms in (2) represent the Hamiltonians for free ion, crystal field and spin-orbit interactions, respectively. The last term represents the effective Hamiltonian which describes the interaction of the Mn^{4+} d^3 electrons with the lattice normal modes of the host crystal.

In the cluster model [27] we will consider the $[MnF_6]^{2-}$ octahedron as a cluster with the a_{1g}, e_g and t_{2g} Jahn–Teller active normal modes. In order to evaluate the constants of the vibronic coupling between these normal modes and the $^4T_{2g}$ electronic state we use the dynamic ligand field model [31, 32]. In the linear approximation of this model the vibronic coupling constants have the following explicit expressions [32]:

$$\left\langle {}^4T_{2g} \left\| \frac{\partial V}{\partial Q_{a_{1g}}} \right\| {}^4T_{2g} \right\rangle = -\frac{50}{\sqrt{6}} \frac{Dq}{R_0}, \quad (3)$$

$$\left\langle {}^4T_{2g} \left\| \frac{\partial V}{\partial Q_{e_g}} \right\| {}^4T_{2g} \right\rangle = -\frac{25}{\sqrt{3}} \frac{Dq}{R_0}, \quad (4)$$

$$\left\langle {}^4T_{2g} \left\| \frac{\partial V}{\partial Q_{t_{2g}}} \right\| {}^4T_{2g} \right\rangle = \frac{4\sqrt{3}}{7} \frac{Dq}{R_0} \left(\frac{5}{3} - \frac{3}{\eta} \right), \quad (5)$$

where $Dq = 2063$ cm^{-1} is the crystal field strength, $R_0 = 1.74$ Å is the equilibrium distance between central ion and ligands, and the parameter η is

$$\eta = \frac{\langle r^4 \rangle}{\langle r^2 \rangle R_0{}^2}. \quad (6)$$

Here $\langle r^4 \rangle$ and $\langle r^2 \rangle$ are the averaged values of the corresponding power of the Mn^{4+} ion electron radial coordinate. This parameter is related to the well known angular overlap model (AOM) parameters e_σ and e_π [33] ($e_\delta \equiv 0$):

$$\eta = \frac{3}{5} \cdot \frac{3 - 4e_\pi/e_\sigma}{1 + e_\pi/e_\sigma}. \quad (7)$$

From a two-dimensional spectrochemical series [34] the ratio of the AOM-parameters e_π and e_σ for $[MnF_6]^{2-}$ is obtained: $e_\pi/e_\sigma \approx 0.31$, and with (7), $\eta \approx 0.8$. Using the values of Dq, R_0 and η, we obtain from (3), (4) and (5)

$$\left\langle {}^4T_{2g} \left\| \frac{\partial V}{\partial Q_{a_{1g}}} \right\| {}^4T_{2g} \right\rangle = -0.48 \cdot 10^{-8} N,$$

$$\left\langle {}^4T_{2g} \left\| \frac{\partial V}{\partial Q_{e_g}} \right\| {}^4T_{2g} \right\rangle = -0.33 \cdot 10^{-8} N,$$

and

$$\left\langle {}^4T_{2g} \left\| \frac{\partial V}{\partial Q_{t_{2g}}} \right\| {}^4T_{2g} \right\rangle = -0.48 \cdot 10^{-9} N.$$

As can be seen, the coupling to the t_{2g} mode is weaker than to the a_{1g} and e_g modes, and the excited state potential energy surface is shifted along the a_{1g} as well as e_g coordinates, the former being somewhat stronger than the latter. Even if the t_{2g}-coupling is smaller, the experimental results from [15, 16] have shown that the t_{2g} mode appears to originate a progression in e_g and possibly a_{1g} with the most intense feature. That is why we will consider the linear $^4T \otimes (e_g + t_{2g})$ coupling case, where the absolute e_g – minima coexist with t_{2g} – saddle points.

According to Wissing and Degen [32], in the title case $\eta > 0.7$ and $\nu_{t_{2g}}/\nu_{e_g} > 0.5$ ($\nu_{t_{2g}} = 266$ cm^{-1} and $\nu_{e_g} = 494$ cm^{-1} [14]) the $^4T_{2g} \otimes e_g$ minima are deeper than the $^4T_{2g} \otimes t_{2g}$ minima, and the cluster $[MnF_6]^{2-}$ distorts only in the tetragonal direction. Taking this conclusion into account, in the next section, dedicated to the geometry of the excited state $^4T_{2g}$ of $Cs_2GeF_6:Mn^{4+}$, we will treat the influence of the a_{1g} and e_g vibronic coupling only with the $^4T_{2g}$ electronic state of Mn^{4+} ions.

Using Avram and Brik's analysis [19, 35] of the Ham quenching of the origin multiplet, we obtain the values in column c of Table 1 (Sect. III) and calculate the Jahn–Teller stabilization energy in the $^4T_{2g}$ state, $E_{JT} = 438$ cm^{-1}. It corresponds to the Jahn–Teller reduction parameter $\lambda = \exp\left(-\frac{3}{2}\frac{E_{sT}}{h\nu_{e_g}}\right) = 0.26$ and a Huang–Rhys factor $S_{e_g} = 0.89$.

5. Geometry of the $^4T_{2g}$ Excited State in $Cs_2GeF_6:Mn^{4+}$

The adiabatic potentials corresponding to the ground and excited states of Mn^{4+} ions in the $[MnF_6]^{2-}$ cluster have different geometries. This leads to a relative displacement of their potential energy surface along the a_{1g} and e_g normal modes of the cluster, as we have carried out in the end of last section.

In order to calculate the equilibrium displacements of the $^4T_{2g}$ from the ground state along the a_{1g} and e_g active modes we use the following equation [36]

$$|\Delta Q_i|_{eq} = \left[\frac{2S_i h\nu_i}{f_i}\right]^{1/2}. \qquad (8)$$

Table 2. Huang–Rhys factors and equilibrium geometries of the $[MnF_6]^{2-}$ octahedron in the $^4T_{2g}$ quartet excited state relative to the $^4A_{2g}$ ground state in Mn^{4+} doped Cs_2GeF_6.

$S_{a_{1g}}$ [a]	2.75	$\lvert\Delta Q_{a_{1g}}\rvert_{eq}$ (Å)	0.16	$\Delta x_{eq}, \Delta y_{eq}$ (Å)	0.09
S_{e_g} [b]	0.89	$\lvert\Delta Q_{e_g}\rvert_{eq}$ (Å)	−0.09	Δz_{eq} (Å)	0.01

[a] From [38]. [b] This paper.

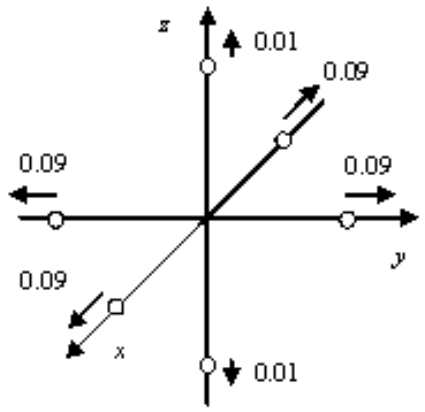

Fig. 1. Distortion of the $[MnF_6]^{2-}$ complex in the $^4T_{2g}$ excited state with respect to the ground state (displacements in Å).

Here Q_i denotes the i^{th} normal mode, with the force constant f_i of the harmonic potential. S_i are the Huang–Rhys factors.

The f_i constants were calculated with the FG matrix method for an octahedral $[MnF_6]^{2-}$ cluster [37]. With $h\nu_{a_{1g}} = 512$ cm^{-1} and $h\nu_{e_g} = 494$ cm^{-1} [13, 14], we obtain $f_{a_{1g}} = 218$ N/m and $f_{e_g} = 203$ N/m, respectively.

The Huang–Rhys factor $S_{e_g} = 0.89$ was calculated at the end of the last section, based on the Ham quenching of the $^4T_{2g}$ spin-orbit splitting due to the dynamical Jahn–Teller effect. The Huang-Rhys factor for vibronic coupling with the normal mode a_{1g} is $S_{a_{1g}} = 2.75$ [38].

Using these data, we got, from (8), $|\Delta Q_{a_{1g}}|_{eq} = 0.16$ Å and $|\Delta Q_{e_g}|_{eq} = 0.09$ Å. As previously demonstrated, based on group theoretical considerations and the $^4T_{2g}$ wave functions [39, 40], the sign of $\Delta Q_{a_{1g}eq}$ is positive, whereas the sign of $\Delta Q_{e_g eq}$ is negative.

Like in [35], the coordinate system in the $(Q_\theta, Q_\varepsilon)$ space can always be chosen in such a way, that the potential minimum of the $^4T_{2g}$ component under consideration (either ξ, η or ζ) lies on the Q_θ axis, i.e. no distortion occurs along Q_ε. Then it is possible to consider the $|\Delta Q_{e_g}|_{eq}$ values as corresponding to $|\Delta Q_{e_{g\theta}}|_{eq}$, whereas $|\Delta Q_{e_{g\varepsilon}}|_{eq}$ is zero. Also, we will use the connection between displacements of normal coordinates

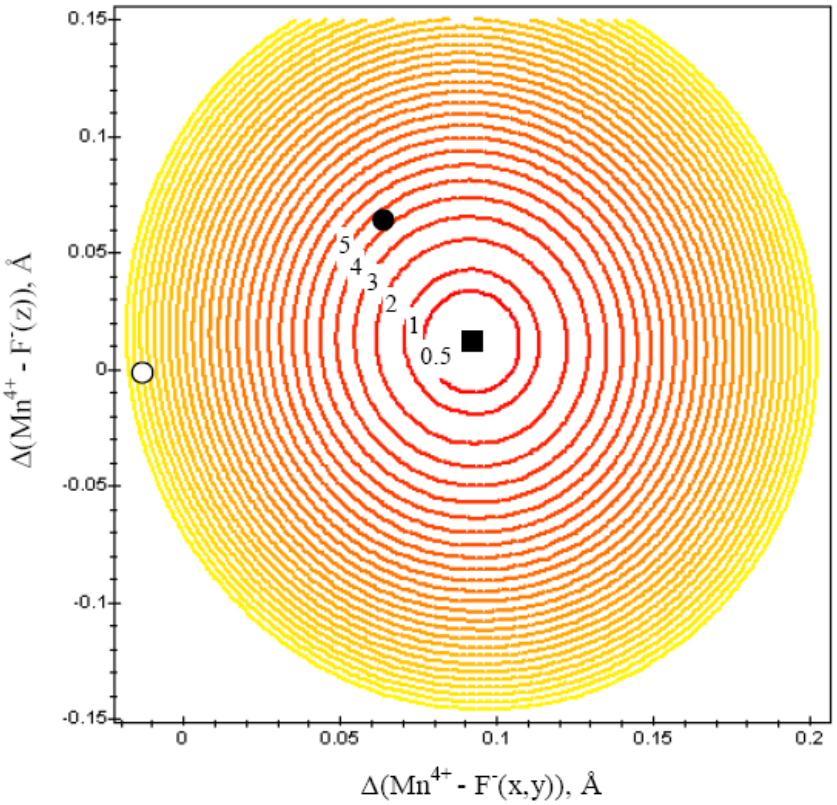

Fig. 2. Contour plot of the harmonic $^4T_{2g}$ potential energy surface for the Cs2GeF$_6$:Mn^{4+} system as a function of changes in the $Mn^{4+} - F^-(x,y)$ and $Mn^{4+} - F^-(z)$ chemical bonds lengths. The energies of individual contours are given in hundreds of wave numbers. The open circle around the origin corresponds to the equilibrium position of the ground $^4A_{2g}$ potential energy surface; the black square indicates the equilibrium position of the $^4T_{2g}$ potential energy surface shifted with respect to the ground state as a combined result of the a_{1g} and e_g normal vibrations. The black circle shows the hypothetical position of the $^4T_{2g}$ potential energy surface minimum if there were no e_g normal vibration (i.e. in the absence of the Jahn–Teller distortion).The value on the potential energy surface of the $^4T_{2g}$ state at this point (between 400 and 500 cm^{-1} in the figure) corresponds to the Jahn–Teller energy for the considered complex. Details of calculations are given in the text.

ΔQ and changes in the metal-ligand bond lengths [39]

$$\begin{pmatrix}\Delta x\\ \Delta y\\ \Delta z\end{pmatrix} = \frac{1}{2}\begin{pmatrix}\sqrt{\frac{2}{3}} & -\sqrt{\frac{1}{3}} & -1\\ \sqrt{\frac{2}{3}} & -\sqrt{\frac{1}{3}} & 1\\ \sqrt{\frac{2}{3}} & -\sqrt{\frac{4}{3}} & 0\end{pmatrix}\begin{pmatrix}\Delta Q_{a_{1g}}\\ \Delta Q_{e_g\theta}\\ \Delta Q_{e_g\varepsilon}\end{pmatrix}. \quad (9)$$

Equation (9) explains why it is convenient to perform a specific rotation of the coordinate system in the $(Q_\theta, Q_\varepsilon)$ space described above: if $|\Delta Q_{e_g\varepsilon}|_{eq} = 0$, then $\Delta x = \Delta y$, and the potential energy surface can be easily visualised. Table 2 contains the Huang–Rhys factors and the equilibrium geometries of the $[MnF_6]^{2-}$ octahedron in the $^4T_{2g}$ first quartet excited state relative to the $^4A_{2g}$ ground state in the Mn^{4+} doped Cs_2GeF_6 crystal.

The combined effect of the a_{1g} and e_g displacements is a net equatorial expansion and a slight axial stretching (Fig. 1).

It should be pointed out, that similar analyses performed for the Cr^{3+} ion in $Cs_2NaYCl_6:Cr^{3+}$ and $Cs_2NaYBr_6:Cr^{3+}$ [20, 22], $Cs_2NaScCl_6:Cr^{3+}$ [23] and $CsCaF_3:V^{2+}$ [35] have lead to a deformation of the opposite sign along the z-axis, namely, to a slight axial contraction, whereas for $CsCaF_3:V^{2+}$ [26] and $Cs_2GeF_6:Mn^{4+}$ we have a slight axial stretching. The criterion, which defines the contraction along the z-axis deformation, is

$$|\Delta Q_{a_{1g}}|_{eq} < |\Delta Q_{e_g}|_{eq}\sqrt{2}. \quad (10)$$

If the above condition is not obeyed, the complex will expand along the *z*-axis.

6. Conclusions

In this paper we have calculated the fine structure of the first excited quartet $^4T_{2g}$ of an Mn^{4+} ion doped in a Cs_2GeF_6 crystal. A theoretical analysis of vibronic interaction, manifested as dynamical Jahn–Teller effect, between the $^4T_{2g}$ state and a_{1g}, e_g, and t_{2g} normal modes of the host matrix, shows that the coupling $^4T_{2g} \otimes (e_g + t_{2g})$ distorts the complex only in the tetragonal direction, and the $^4T_{2g} \otimes e_g$ minima are deeper than the $^4T_{2g} \otimes t_{2g}$ minima. Our model calculations show that the excited state potential energy surface $^4T_{2g}$ is shifted along the a_{1g} as well as e_g coordinates, the former being somewhat stronger than the latter. The combined coupling of the $^4T_{2g}$ electronic state of the Mn^{4+} ion to the a_{1g} and e_g normal modes gave a possibility for estimation of the equilibrium displacements of the ligands. It is shown that the net result of both vibrations is a net equatorial expansion and a slight axial stretching, opposite to the case of trivalent chromium ions in different hosts. The Jahn–Teller stabilization energy $E_{JT} = 439.6\ cm^{-1}$ has been estimated from the contour plot of the potential surface energy in the $^4T_{2g}$ electronic state (Fig. 2). This result agrees well with results obtained from the Ham theory for this case.

Acknowledgements

The author M. G. Brik is financially supported by the Japanese Ministry of Education, Culture, Sports, Science and Technology (MEXT) in a project on computational materials science at Kyoto University.

[1] R. C. Powell, Physics of Solid-State Laser Materials, Springer, Berlin 1998.
[2] S. Kück, Appl. Phys. B **72**, 515 (2001).
[3] S. Sugano, Y. Tanabe, and H. Kamimura, Multiplets of Transition-Metal Ions in Crystals, Academic Press, New York 1970.
[4] I. B. Bersuker, Electronic Structure and Properties of Transition Metal Compounds. Introduction to the Theory, Wiley, New York 1996.
[5] N. P. Barnes in Tunable Lasers Handbook, Ed. F. J. Duarte, Academic Press, New York 1995, pp. 219.
[6] B. Henderson and R. H. Bartram, Crystal-Field Engineering of Solid-State Laser Materials, Cambridge University Press, Cambridge 2000.
[7] W. Knierim, A. Honold, U. Brauch, and U. Dürr, J. Opt. Soc. Amer. **B3**, 119 (1986).
[8] U. Brauch and U. Dürr, Opt. Commun. **55**, 35 (1985).
[9] U. Dürr and U. Brauch, in Tunable Solid-State Lasers II, Eds. A. B. Budgor, L. Esterowitz, and L. G. De Shazer, Springer, Berlin 1986.
[10] J. A. Caird, in Tunable Solid-State Lasers II, (eds. A. B. Budgor, L. Esterowitz, and L. G. De Shazer), Springer, Berlin 1986, pp.20.
[11] B. Henderson and G. F. Imbush, Contemp. Phys. **29**, 235 (1988).
[12] A. A. Kaminskii, Phys. Stat. Sol. (a) **200**, 215 (2003).
[13] S. L. Chodos, M. M. Black, and C. D. Flint, J. Chem. Phys. **65**, 4816 (1976).
[14] L. Helmholz and M. E. Russo, J. Chem. Phys. **59**, 5455 (1973).
[15] R. L. Chien, J. M. Berg, D. S. McClure, P. Rabinowitz, and B. N. Perry, J. Chem. Phys. **84**, 4168 (1986).
[16] C. Campochiaro, D. S. McClure, P. Rabinowitz, and S. Dougal, Chem. Phys. Lett. **157**, 78 (1989).
[17] M. D. Sturge, Phys. Rev. **B1**, 1005 (1970).
[18] G. Bevilacqua, L. Martinelli, and E. E. Vogel, Phys. Rev. **B66**, 155338 (2002).
[19] C. N. Avram and M. G. Brik, J. Lumin. **108**, 319 (2004).
[20] H. U. Güdel and T. R. Snellgrove, Inorg. Chem. **17**, 1617 (1978).
[21] O. Pilla, E. Galvanetto, M. Montagna, and G. Viliani, Phys. Rev. **38**, 3477 (1988).
[22] R. Knochenmuss, C. Reber, M. V. Rajasekharan, and H. U. Güdel, J. Chem. Phys. **85**, 4280 (1986).
[23] O. S. Wenger and H. U. Güdel, J. Chem. Phys. **114**, 5832 (2001).
[24] C. N. Avram and M. G. Brik, J. Lumin. **102 – 103**, 81 (2003).
[25] F. S. Ham, Phys. Rev. **6A**, 1727 (1965).
[26] C. N. Avram, M. G. Brik, I. Tanaka, and N. M. Avram, Physica B, in press. doi:10.1016/j.physb.2004.10.052
[27] M. D. Sturge, in Advanced in Solid State Physics, Vol. 20, (Eds. F. Seitz, D. Turnbull, and H. Ehrenreich), Academic Press, New York 1967, pp. 91.
[28] J. C. Eisenstein, J. Chem. Phys. **34**, 1628 (1961).
[29] J. S. Griffith, The Theory of Transition Metal Ions, Cambridge University Press, Cambridge 1972.
[30] J. Kanamori, Progr. Theoret. Phys. (Kyoto) **17**, 177 (1957).
[31] H. H. Schmidtke and J. Degen, Structure and Bonding **71**, 99 (1989).
[32] K. Wissing and J. Degen, Mol. Phys. **95**, 51 (1998).
[33] M. Kibler, Aust. J. Chem. **35**, 231 (1982).

[34] T. Schönherr, Topics Current Chem. **191**, 87 (1997).
[35] M. G. Brik, N. M. Avram, and I. Tanaka, Phys. Stat. Sol. (b) **241**, 2982 (2004); DOI 10.1002/pssb.20040289.
[36] T. C. Brunold and H. U. Güdel, in Inorganic Electronic Structure and Spectroscopy, Vol. I: Methodology, Eds. E. I. Solomon and A. B. P. Lever, John Wiley & Sons, Inc, New York 1989.
[37] K. Venkateswarlu and S. Sundaram, Phys. Chem. N. Folge **9**, 174 (1956).
[38] L. Seijo, Z. Barandiaran, and D. S. McClure, Int. J. Quantum Chem. **80**, 623 (2000).
[39] E. I. Solomon and D. S. McClure, Phys. Rev. **B9**, 4690 (1974).
[40] R. B. Wilson and E. I. Solomon, Inorg. Chem. **17**, 1729 (1978).